IMAGE DOMAIN SCATTERING CENTER MODELS FOR SYNTHETIC APERTURE RADAR

Michael J. Gerry, Lee C. Potter, Randolph L. Moses and Michael A. Koets

Department of Electrical Engineering
The Ohio State University
Columbus, OH 43210

ABSTRACT

We present a parametric model to describe radar scattering of man-made objects from synthetic aperture radar (SAR) measurements. The model is developed for high frequency scattering of objects in the frequency-angle domain, and transformed into the image domain for parameter estimation. The image-domain model is applied to SAR image segments to extract a geometrically relevant parametric description of dominant scattering behavior. The estimated parameters provide a concise description of the measured scattering, and has applications in object recognition and data compression.

1. INTRODUCTION

In this paper we develop a two-dimensional model for radar scattering that is useful for describing high frequency synthetic aperture radar measurements of objects. The model is based on a scattering center description of the objects of interest; at high frequencies, the scattering response of an object is well approximated as a sum of responses from individual scattering centers [1]. These scattering centers provide a concise, physically relevant description of the object and are thus good candidates for use in target recognition, radar data compression, and scattering phenomenology studies.

We develop a two-dimensional model for radar scattering as a function of frequency and aspect. The model is based on the physical optics and the geometric theory of diffraction (GTD) monostatic scattering solutions. It extends the one-dimensional GTD model presented in [2] to include aspect angle, and extends the two-dimensional model in [3] to more physically relevant parameterizations. The model provides a physical description of target scattering centers, each of which is described by a set of parameters characterizing position, shape, orientation (pose) and amplitude. This is a richer description of target scattering than is available either from conventional Fourier-based imaging techniques [4] or from less physically accurate point scattering parametric models [5]. The aspect dependence in our two-dimensional model allows description of both localized and distributed scattering centers, providing a higher fidelity description of scattered fields.

The model is derived in the frequency-angle domain, but transformed into the image domain where it is applied to measured SAR image data. Image-domain processing affords a number of advantages, including computational efficiency, insertion into standard SAR processing streams, and robustness to noise and clutter. In most SAR applications, imaging of the measured data is the first step carried out, and subsequent data processing (*e.g.*, for target detection and recognition) is applied to image-domain data. Data compression and scattering phenomenology studies also benefit from image-domain processing and interpretation. Finally, image-domain processing provides robustness to clutter model assumptions, and permits isolating regions of high signal-to-clutter ratios for model fitting [5, 3].

We present an algorithm for estimating the model order and model parameters from a measured SAR image. The algorithm recursively estimates and subtracts modeled terms from the data until the residual energy is below a user-selected threshold. At each step, the scattering center parameters are estimated on a segmented region of the image using a nonlinear least squares minimization procedure. Numerical examples presented for measured data show the effectiveness of the algorithm, with parameter estimation accuracy achieving the Cramér-Rao bound.

This work was sponsored by the Defense Advanced Research Projects Agency under grant number FF33615-97-1-1020.

2. SCATTERING MODEL

We first develop a parametric model for the backscatter from objects measured as a function of frequency and aspect angle (see also [6]). We seek a model that maintains high fidelity to the scattering physics for many objects, yet is sufficiently simple in its functional form to permit robust inference from estimated parameters. We then transform the model through SAR image processing procedures to arrive at an image-domain scattering model.

2.1. Frequency Domain Model

We assume a data collection scenario in which a frequency diverse radar measures the scattered field of an object at a number of different aspect angles ϕ. At high frequencies, the total scattered field can be written as a sum of p individual scattering terms:

$$E^s(f,\phi) = \sum_{n=1}^{p} E_n^s(f,\phi) \tag{1}$$

Assuming far-field scattering, most scattering centers exhibit linear phase dependence with frequency (the restriction to linear phase scatterers excludes phase dispersive scattering mechanisms such as resonant cavities and creeping waves), so

$$E_n^s(k,\phi) = S_n(k,\phi)\exp\{j2k\hat{r}\cdot\vec{r}_n\} \tag{2}$$

where $k = 2\pi f/c$ is the wave number, f is frequency in Hertz, c is the propagation velocity, ϕ is the aspect angle, $\hat{r}$ is the unit vector in the direction of the scattered field, and $\vec{r}_n = [x_n, y_n]$ is the position vector of the nth scattering center projected to the plane. Thus, the phase dependence of our model describes the location of each scattering center in the plane of the radar measurement.

The amplitude term $S_n(f,\phi)$ is a slowly varying function. At high frequencies, amplitude dependence on frequency is well-modeled by the geometric theory of diffraction (GTD), and is proportional to $(jk)^\alpha$, where α takes on half integer values that relate to the geometry of the scattering center [7, 8] (see Table 1).

As aspect angle ϕ varies, we assume that the scattering center behaves in one of two ways: either it is localized and appears to exist in a single point in space, or it is distributed in space and appears as a finite, nonzero length current distribution. Examples of localized scattering mechanisms are trihedral reflection, corner diffraction, and edge diffraction. All of these mechanisms have slowly varying amplitude as a function of aspect angle. We exploit the commonality of localized mechanisms by modeling this slowly varying function with a damped exponential

Table 1: Alpha values for canonical scatterers.

α	Example scattering geometries
1	flat plate at broadside; dihedral
$\frac{1}{2}$	singly curved surface reflection
0	point; sphere; straight edge specular
$-\frac{1}{2}$	edge diffraction
-1	corner diffraction

$$S_n(f,\phi) = A_n\exp(-2\pi f\gamma_n\sin\phi) \tag{3}$$

The exponential function provides a mathematically convenient approximation containing only a single parameter. Although physical insight is used to arrive at the exponential model, the parameter γ_n has no direct physical interpretation. Examples of distributed scattering mechanisms are flat plate reflection, dihedral reflection, and cylinder reflection. Each of these scattering mechanisms has an amplitude dependence on aspect angle that is dominated by a $\mathrm{sinc(x)} = \frac{\sin(x)}{x}$ function. We thus adopt the sinc(x) function to characterize angle dependence in the scattering model for scattering centers that are distributed:

$$S_n(f,\phi) = A_n\mathrm{sinc}\left(kL_n\sin(\phi-\phi_n)\right) \tag{4}$$

where L_n is the length and ϕ_n is the orientation angle of the distributed scatterer.

Combining the above dependencies, we find that $E_n^s(f,\phi)$ is modeled as one of the two following functions:

$$\begin{aligned} E_n^s(f,\phi) &= A_n\left(j\frac{f}{f_c}\right)^{\alpha_n}\mathrm{sinc}\left(\frac{2\pi f}{c}L_n\sin(\phi-\phi_n)\right) \\ &\quad\cdot\exp\left(-j\frac{4\pi f}{c}(x_n\cos\phi+y_n\sin\phi)\right) \end{aligned} \tag{5}$$

$$\begin{aligned} E_n^s(f,\phi) &= A_n\left(j\frac{f}{f_c}\right)^{\alpha_n}\exp(-2\pi f\gamma_n\sin\phi) \\ &\quad\cdot\exp\left(-j\frac{4\pi f}{c}(x_n\cos\phi+y_n\sin\phi)\right) \end{aligned} \tag{6}$$

where the first model corresponds to a distributed scattering center and the second model corresponds to a localized scattering center. Inserting equations (5) and (6) into equation (1) gives a scattering model that is described by the parameter set $\{A_n, x_n, y_n, \alpha_n\}$, along with either γ_n or $\{\phi_n, L_n\}$, for $n = 1, ..., p$. The parameters provide a rich physical description of the scatterers that are present in the data set. The model is based

on scattering physics and is developed to describe a large class of scatterers while still maintaining a relatively simple form.

2.2. Image Domain Model

Measured radar data collected as a function of frequency and aspect is nearly always processed coherently to form an image for display and interpretation. While several variations of image formation are used, a common approach is to transform the frequency-angle measurements to a rectangular grid, shift to baseband, window and zero pad, and perform a two-dimensional inverse Fourier transform. This yields a complex-valued baseband image (*i.e.*, with the radar center frequency modulation suppressed) in the (x, y) domain. Image formation is one of the first steps in SAR processing, and it is common that only the image-domain data available to subsequent processing steps. For this and other reasons discussed below, we are motivated to transform our scattering model to the image domain for parameter estimation.

The image domain provides several advantages for estimation of the unknown parameters. First is clutter suppression; much of the unwanted scattering energy is in the form of backscatter from clutter in the scene. Desired scattering terms have responses whose energies are localized in the image plane and clutter is often localized away from the scattering of interest (for example, it could come from a tree near the object). Desired responses can thus be isolated from clutter by segmenting the image and applying parameter estimators to segmented subsets of the image. In addition, we can assume that each segmented region is electrically isolated from other such regions, so we can process regions in parallel using low local model orders that describe the the number of scattering centers in the region only. Image domain processing of each peak region thus reduces computational complexity. Finally, image domain processing allows insertion of the model-based scattering analysis into a multi-staged automatic target recognition algorithm. The model-based scattering analysis is performed only after a computationally inexpensive prescreening stage [9], at which point typically only SAR image "chips" in regions of interest are available to algorithms.

We have transformed the model given by equations (1)–(6) through the SAR image formation steps outlined above. The transformation process is straightforward but tedious and yields lengthy expressions which we omit here; details are given in [10]. In doing so, we require that the window function is separable in the rectangular frequency dimensions f_x and f_y, and that it is expressible as a sum of complex exponentials; many commonly used window functions, such as rectangular, Hamming, Hanning, and Taylor windows satisfy this restriction.

3. PARAMETER ESTIMATION

In this section we present an approximate Maximum Likelihood (ML) technique for estimating the parameters of the image domain scattering model. For each of p scattering centers, there are six or seven real-valued parameters to be estimated, depending on whether equation (5) or (6) is used: the amplitude and phase, A_n, frequency damping r_n, aspect damping γ_n or length L_n and tilt angle ϕ_n, down range position x_n, and cross range position y_n. In addition, for each scattering center we have the binary decision of whether to use the scattering model corresponding to equation (5) or equation (6). Finally, we must address order selection.

The algorithm we use a recursive CLEAN-type algorithm that successively models scattering centers, then subtracts the modeled component from the data. At each stage, the initial step is to segment from the image its highest energy region; we use a "water filling" algorithm presented in [11]. We combine adjacent regions if their minimum amplitude is close to the region maximum values; this effectively forms a single region for distributed scattering centers. We next apply an *ad hoc* test, based on the shape of the region, to decide whether to use a localized or isolated scattering model (*i.e.*, equation (5) or (6)). We then estimate the model parameters by minimizing the squared error between the model and the measured image domain data

$$J(\Theta) = \sum_{pixels} |\text{image chip} - \text{model}(\Theta)|^2 \qquad (7)$$

over the pixels in the identified region only; here Θ is a vector containing the parameters to be estimated and model(Θ) is the image-domain analog of equation (5) or (6). An iterative optimization procedure is used to minimize $J(\Theta)$. There are many nonconvex optimization procedures in the literature, and we choose to use the simplex downhill method.

Once the parameter estimates have been obtained, we compute the contribution of the estimated scattering center on the entire image domain and subtract it from the data. We then test the energy in the residual, and if it is above a predefined threshold, we apply the entire segmentation and estimation procedure to the residual data. The process continues recursively until the residual energy is sufficiently small. At the conclusion, the above algorithm yields estimates of scattering parameters that describe the position, size, shape and

orientation of the scattering centers that comprise the measured target.

We note that the least squares cost function in equation (7) is nonconvex with many local minima. Therefore, initialization is important, and robustness is improved by using low model orders on small segments of the data. Initialization of range and cross range positions is computed from local maxima in the image chip, while r_n and γ_n are initialized at zero (point scattering). We presently restrict the model order to one for each image segment, which works well for well-separated scattering mechanisms; of course, higher model orders could also be considered.

4. EXAMPLES

We present a measured target example which illustrates the effectiveness of our image domain model at compressing large measured data sets into a small set of physically descriptive parameters. These parameters describe the shape, position, and orientation of scattering centers comprising the target response over the measured frequency and angle spans.

First we consider the scattering from a square flat plate measured in the Ohio State University Electro-Science Laboratory (ESL) Compact Range [12]. We analyze stepped frequency measurements of the plate for frequencies 9.5–10.5 GHz in 20MHz steps and for angles ± 3 degrees (in 0.5 degree steps) from broadside to one of the edges. The plate is a two foot square and lies in the plane of rotation. The measurement polarization is horizontal.

Figure 1 shows an image of the plate. The image contains three dominant scattering centers. The broadside response of the edge of the plate appears as a line in the image. The two remaining corners on the back of the plate appear as point mechanisms. The algorithm of Section 3 is used to estimate the number of scattering centers, their type, and the corresponding parameters. The algorithm correctly estimates the scattering type, its frequency dependence parameters ($\alpha = 0$ for the front edge and $\alpha = -1$ for the corners), and estimates the location and length to within the accuracy of the truth data. The residual squared error between the measured data and the three-scatterer model reconstruction is 2.88%.

To assess parameter uncertainty, Figure 2 compares the estimated parameters with their Cramér-Rao bounds (derived in [6]). For this figure, we added Gaussian white noise with different noise variances to the measured data, and applied the above estimation algorithm. For each noise variance we obtained estimates of the scattering parameters from 50 Monte-Carlo sim-

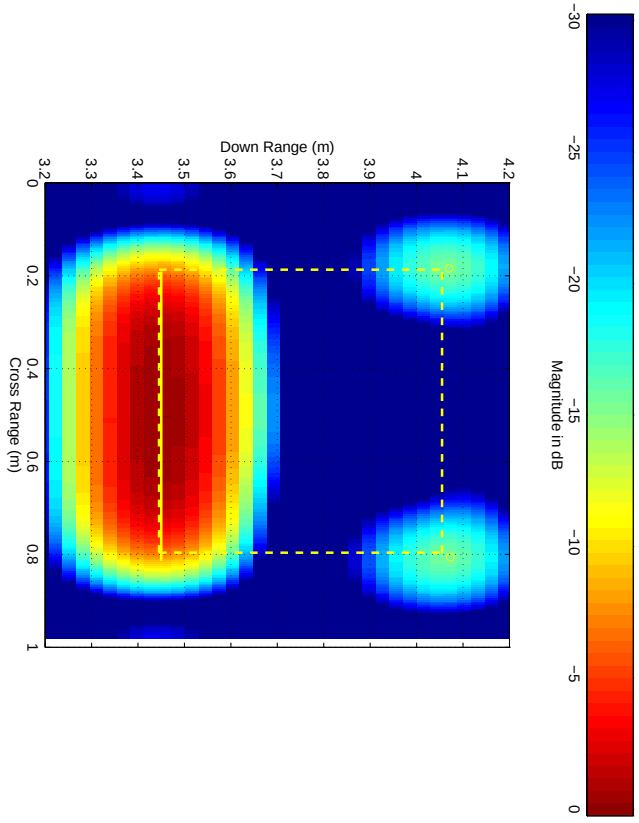

Figure 1: Image and estimates for plate example

ulations, and Figure 2 compares the estimated variance to the corresponding Cramér-Rao bounds for five parameters corresponding to the front edge. We see very good agreement between the CRB and simulation using measured data, which gives confidence that the CRB is a useful tool for performance prediction for our model and algorithm.

5. CONCLUSIONS

We presented a parametric scattering model based on physical scattering center theory. The model balances physical fidelity with simplicity in functional form to yield small modeling error using a small model order with physically relevant parameters. The model is transformed to the image domain, where the parameters are estimated using nonlinear least squares on image segments. The image domain processing affords robustness to noise and clutter, computational savings by subdividing the estimation problem into smaller problems of lower model order, and facilitates insertion into an automatic target recognition processing stream in which later processing stages operate on small image chips identified as regions of interest from earlier pro-

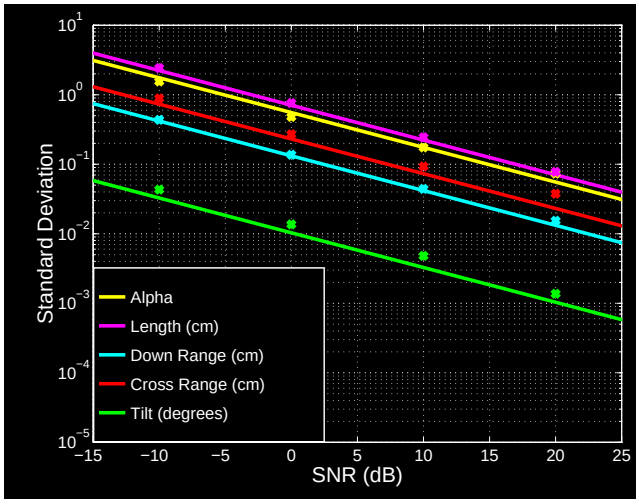

Figure 2: Comparison of Monte-Carlo simulation variance estimates to Cramér-Rao bounds for five parameters corresponding to the front edge plate scattering center.

cessing stages. The algorithm recursively estimates model order, and autonomously chooses between localized and distributed scattering mechanisms. Experiments using measured data, and comparisons of simulation variances with the Cramér-Rao bound, give promising results.

6. REFERENCES

[1] J. B. Keller, "Geometrical Theory of Diffraction," *J. Opt. Soc. Am.*, vol. 52, pp. 116–130, 1962.

[2] L. C. Potter, D.-M. Chiang, R. Carrière, and M. J. Gerry, "A GTD-based parametric model for radar scattering," *IEEE Transactions on Antennas and Propagation*, vol. 43, pp. 1058–1067, October 1995.

[3] Joseph J. Sacchini, *Development of Two--Dimensional Parametric Radar Signal Modeling and Estimation Techniques with Application to Target Identification*. PhD thesis, The Ohio State University, Columbus, OH, 1992.

[4] D.L. Mensa, *High-Resolution Radar Cross Section Imaging*. Boston, MA: Artech House, 1991.

[5] M.-W. Tu, I.J. Gupta and E.K. Walton, "Application of Maximum Likelihood Estimation to Radar Imaging," *IEEE Transactions on Antennas and Propagation*, vol. 45, pp. 20–27, January 1997.

[6] M. J. Gerry, L. C. Potter, I. J. Gupta, and A. van der Merwe, "A parametric model for synthetic aperture radar measurements," *IEEE Transactions on Antennas and Propagation*. (submitted April 1997).

[7] M. A. Plonus, R. Williams and S. C. H. Wang, "Radar Cross Section of Curved Plates Using Geometrical and Physical Diffraction Techniques," *IEEE Transactions on Antennas and Propagation*, vol. 26, pp. 488–493, May 1978.

[8] R.A. Ross, "Radar Cross Section of Rectangular Flat Plates as a Function of Aspect Angle," *IEEE Transactions on Antennas and Propagation*, vol. 14, pp. 329–335, May 1966.

[9] L. M. Novak, G. J. Owirka, and C. M. Netishen, "Performance of a High-Resolution Polarimetric SAR Automatic Target Recognition System," *The Lincoln Laboratory Journal*, vol. 6, pp. 11–24, November 1993.

[10] Michael J. Gerry, *Two-Dimensional Inverse Scattering Based on the GTD Model*. PhD thesis, The Ohio State University, Columbus, OH, 1997.

[11] J. Stach and E. LeBaron, "Enhanced Image Editing by Peak Region Segmentation," *Proceedings of 1996 AMTA Symposium*, October 1996.

[12] E.K. Walton and J.D. Young, "The Ohio State University Compact Radar-Cross Section Measurement Range," *IEEE Transactions on Antennas and Propagation*, vol. 32, pp. 1218–1223, November 1984.